

Adversarial Attacks on Uncertainty Enable Active Learning for Neural Network Potentials

Daniel Schwalbe-Koda,^{*)} Aik Rui Tan,^{*)} and Rafael Gómez-Bombarelli^{†)}

Department of Materials Science and Engineering, Massachusetts Institute of Technology, Cambridge, MA 02139

(Dated: 23 December 2024)

Neural network (NN)-based interatomic potentials provide fast prediction of potential energy surfaces with the accuracy of electronic structure methods. However, NN predictions are only reliable within well-learned training domains, with unknown behavior when extrapolating. Uncertainty quantification through NN committees identify domains with low prediction confidence, but thoroughly exploring the configuration space for training NN potentials often requires slow atomistic simulations. Here, we employ adversarial attacks with a differentiable uncertainty metric to sample new molecular geometries and bootstrap NN potentials. In combination with an active learning loop, the extrapolation power of NN potentials is improved beyond the original training data with few additional samples. The framework is demonstrated on multiple examples, leading to better sampling of kinetic barriers and collective variables without extensive prior data on the relevant geometries. Adversarial attacks are new ways to simultaneously sample the phase space and bootstrap NN potentials, increasing their robustness and enabling a faster, accurate prediction of potential energy landscapes.

I. INTRODUCTION

Recent advances in machine learning (ML) techniques have enabled the study of increasingly larger and more complex materials systems.^{1–6} In particular, ML-based atomistic simulations have demonstrated predictions of potential energy surfaces (PESes) with accuracy comparable to *ab initio* simulations while being orders of magnitude faster.^{7–12} ML potentials employing kernels or Gaussian processes have been widely used for fitting PESes,^{13–22} and are particularly effective in low-data regimes. For systems with greater diversity in chemical composition and structures, larger training datasets are typically needed. While Gaussian processes are encumbered by training and inference costs with large amounts of data,²³ neural networks (NNs) can fit interatomic potentials to extensive datasets with high accuracy and constant inference time.²⁴ Over the last years, several models combined different representations and NN architectures to predict PESes with increasing accuracy.^{24–32} They have been applied to predict molecular systems,^{33–36} solids,^{37–39} interfaces,^{26,40} chemical reactions,^{41,42} kinetic events,^{43,44} phase transitions^{45,46} and many more.^{4,7,12}

Despite their remarkable capacity to interpolate between data points, NNs are known to perform poorly outside of their training domain^{47,48} and may fail catastrophically for rare events, such as those occurring at large sizes or time scales rarely explored in the training data. Increasing the amount and diversity of the training data is beneficial to improve performance,^{42,49} but there are significant costs associated to generating new ground-truth data points. Continuously acquiring more

data may negate some of the acceleration provided by ML models. In addition, exhaustive exploration or data augmentation of the input space is intractable. Therefore, assessing the trustworthiness of NN predictions and systematically improving them is fundamental for deploying ML-accelerated tools to real world applications, including the prediction of materials properties.

Quantifying model uncertainty then becomes key, since it allows distinguishing new inputs, which are likely to be informative and worth labeling with *ab initio* simulations, from those close to configurations already represented in the training data. In this context, epistemic uncertainty — the model uncertainty arising from the lack of appropriate training data — is much more relevant to ML potentials than the aleatoric uncertainty, which arises from noise in the training data. Whereas ML-based interatomic potentials are becoming increasingly popular, uncertainty quantification applied to atomistic simulations is at earlier stages.^{50–53} ML potentials based on Gaussian processes are Bayesian in nature, and thus benefit from an intrinsic error quantification scheme, which has been applied to train ML potentials on-the-fly^{22,54} or to accelerate nudged elastic band (NEB) calculations.⁵⁵ NNs do not typically handle uncertainty natively and it is common to use approaches that provide distributions of predictions to quantify epistemic uncertainty. Strategies such as Bayesian NNs,⁵⁶ Monte Carlo dropout⁵⁷ or NN committees^{58–61} allow estimating the model uncertainty by building a set of related models and comparing their predictions for a given input. In particular, NN committee force fields have been used to control simulations,^{62,63} to inform sampling strategies⁶⁴ and to calibrate error bars for computed properties.⁶⁵

Even when uncertainty estimates are available to distinguish informative from uninformative inputs, ML potentials rely on atomistic simulations to generate new trial configurations. For example, it is common to per-

^{*)}D.S.-K. and A.R.T. contributed equally to this work

^{†)}Electronic mail: rafagb@mit.edu

form molecular dynamics (MD) simulations with NN-based models to expand their training set in an active learning (AL) loop.^{42,49,66} Since MD simulations explore the phase space based on the thermodynamic probability of the PES, ML-accelerated MD results in outputs correlated to the training set if the ML potential accurately reproduces the ground truth PES. However, exploring this region only provides incremental improvement to the potentials, which will still struggle to observe rare events. Furthermore, MD trajectories can be unstable when executed with an NN potential, especially in early stages of the AL cycle when the NN training set is not representative of the configuration space. Yet, performing *ab initio* MD to gather data can be excessively costly. Some works avoid performing dynamic simulations, but still require forward exploration of the PES to find new training points.⁶⁷ Hence, one of the major bottlenecks for scaling up NN potentials is minimizing their extrapolation errors until they achieve self-sufficiency to perform atomistic simulations within the full phase space they will be used in, including handling rare events. Inverting the problem of exploring the configuration space with NN potentials would allow for a more efficient sampling of transition states and dynamic control.^{68,69}

In this work, we propose an inverse sampling strategy for NN-based atomistic simulations by performing gradient-based optimization of a differentiable uncertainty metric. Building on the concept of adversarial attacks from the ML literature,^{70,71} new molecular conformations are sampled by backpropagating atomic displacements to find local optima that maximize the uncertainty of an NN committee while balancing thermodynamic likelihood. These new configurations are then evaluated using atomistic simulations (e.g. density functional theory or force fields) and used to retrain the NNs in an AL loop. The technique is able to bootstrap training data for NN potentials starting from few configurations, improve their extrapolation power, and efficiently explore the configuration space. The approach is demonstrated in several atomistic systems, including finding unknown local minima in a PES, improving kinetic barrier predictions for nitrogen inversion, increasing the stability of MD simulations in molecular systems, and sampling of collective variables in alanine dipeptide. This work provides a new method to explore potential energy landscapes without the need for brute-force *ab initio* MD simulations to propose trial configurations.

II. THEORY

A. Neural network potentials

An NN potential is a hypothesis function h_θ that predicts a real value of energy $\hat{E} = h_\theta(X)$ for a given input atomistic configuration X . X is generally described by n atoms with atomic numbers $\mathbf{Z} \in \mathbb{Z}_+^n$ and nuclear coordinates $\mathbf{R} \in \mathbb{R}^{n \times 3}$. Atomic forces F_{ij} on atom i and

cartesian coordinate j are obtained by differentiating the output energy with respect to the atomic coordinates r_{ij} ,

$$\hat{F}_{ij} = -\frac{\partial \hat{E}}{\partial r_{ij}}. \quad (1)$$

The parameters θ are trained to minimize the expected loss given the distribution of ground truth data (X, E, \mathbf{F}) according to the dataset \mathcal{D} ,

$$\min_{\theta} \mathbb{E}_{(X, E, \mathbf{F}) \sim \mathcal{D}} [\mathcal{L}(X, E, \mathbf{F}; \theta)]. \quad (2)$$

During training, the loss \mathcal{L} is usually computed by taking the average mean squared error of the predicted and target properties within a batch of size N ,

$$\mathcal{L} = \frac{1}{N} \sum_{i=1}^N \left[\alpha_E \|E_i - \hat{E}_i\|^2 + \alpha_F \|\mathbf{F}_i - \hat{\mathbf{F}}_i\|^2 \right], \quad (3)$$

where α_E and α_F are coefficients indicating the trade-off between energy and force-matching during training.²⁸ The training proceeds using stochastic gradient descent-based techniques.⁷²

B. Uncertainty quantification

To create a differentiable metric of uncertainty, NN committees are typically implemented by training different h_θ and obtaining a distribution of predictions for each input X . For example, given M models implementing $\hat{E}^{(m)} = h_\theta^{(m)}(X)$, the mean and the variance of the energy of an NN potential ensemble can be computed as

$$\bar{E}(X) = \frac{1}{M} \sum_{m=1}^M \hat{E}^{(m)}(X), \quad (4)$$

$$\sigma_E^2(X) = \frac{1}{M-1} \sum_{m=1}^M \|\hat{E}^{(m)}(X) - \bar{E}(X)\|^2, \quad (5)$$

and similarly for forces,

$$\bar{\mathbf{F}}(X) = \frac{1}{M} \sum_{m=1}^M \hat{\mathbf{F}}^{(m)}(X), \quad (6)$$

$$\sigma_F^2(X) = \frac{1}{M-1} \sum_{m=1}^M \left[\frac{1}{3n} \sum_{i,j} \|\hat{F}_{ij}^{(m)}(X) - \bar{F}_{ij}(X)\|^2 \right]. \quad (7)$$

Whereas the training objective (2) rewards approaching mean energies or forces to their ground truth values, this is not guaranteed for regions outside of the training set.

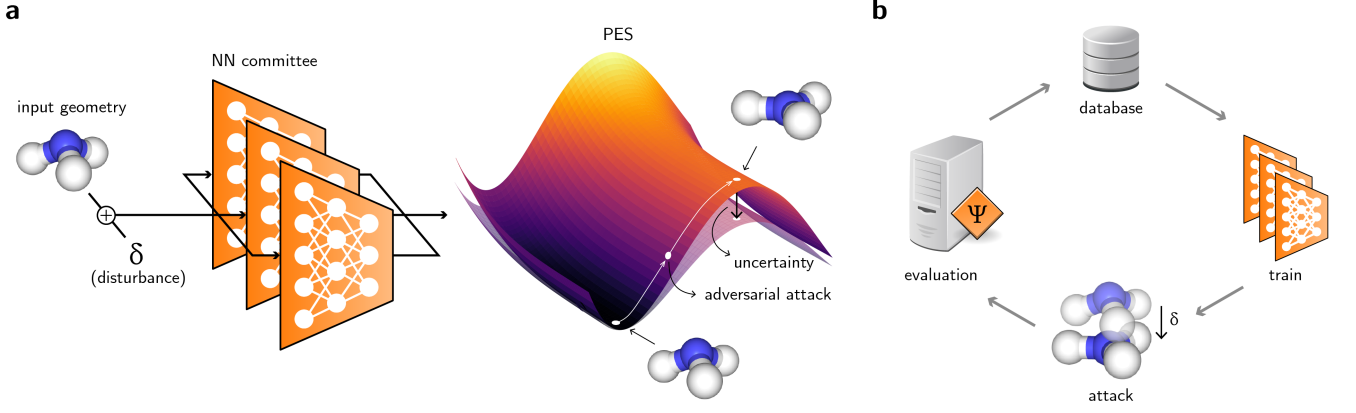


FIG. 1. **a**, Schematic diagram of the method. Nuclear coordinates of an input molecule are slightly displaced by δ . Then, a potential energy surface (PES) and its associated uncertainty are calculated with an NN potential committee. By backpropagating an adversarial loss through the NN committee, the disturbance δ can be updated using gradient ascent techniques until the PES uncertainty is maximized, thus sampling states that compromise high uncertainty with low energy. **b**, Schematic diagram of the active learning loop used to train the NN potential committee. The evaluation can be performed with classical force fields or electronic structure methods.

Since variances in properties may become higher when the NN models are in the extrapolation regime, identifying whether an NN committee is outside its fitting domain requires evaluating the probability that the output of the NN is reliable for an input X . One option is to model this problem for the epistemic error as a simple classifier,

$$P(X \in \mathcal{D} | \sigma^2) = \begin{cases} 1, & \sigma^2 < t, \\ 0, & \sigma^2 \geq t, \end{cases} \quad (8)$$

with t a threshold chosen by evaluating the model on the training set. Although Eq. (8) can be modified to accept the data X with a certain likelihood, the deterministic classifier demonstrates reasonable accuracy despite its simplicity (see Supporting Information for details).

C. Adversarial training

When developing adversarially robust models, the objective (2) is often changed to include a perturbation δ ,⁷³

$$\min_{\theta} \mathbb{E}_{(X, E, \mathbf{F}) \sim \mathcal{D}} \left[\max_{\delta \in \Delta} \mathcal{L}(X_{\delta}, E_{\delta}, \mathbf{F}_{\delta}; \theta) \right], \quad (9)$$

with Δ the set of allowed perturbations and $X_{\delta}, E_{\delta}, \mathbf{F}_{\delta}$ the perturbed geometries and their corresponding energies and forces, respectively. In the context of NN classifiers, Δ is often chosen as the set of ℓ_p -bounded perturbations for a given ε , $\Delta = \{\delta \in \mathbb{R} \mid \|\delta\|_p \leq \varepsilon\}$. Adversarial examples are then constructed by keeping the target class constant under the application of the adversarial attack.^{71,74} On the other hand, adversarial examples are

not well defined for NN regressors. Since even slight variations of the input lead to different ground truth results $E_{\delta}, \mathbf{F}_{\delta}$, creating adversarially robust NN regressors is not straightforward.

We propose that creating adversarially-robust NN potentials can be achieved by combining adversarial attacks, uncertainty quantification, and active learning. Although similar strategies have been used in classifiers and graph-structured data,^{75–77} no work has yet connected these strategies to sample potential energy landscapes. In this framework, an adversarial attack maximizes the uncertainty in the property under prediction (Fig. 1a). Then, ground-truth properties are generated for the adversarial example. This could correspond to obtaining energies and forces for a given conformation with density functional theory (DFT) or force fields approaches. After acquiring new data points, the NN committee is retrained. New rounds of sampling can be performed until the test error is sufficiently low or the phase space is explored to a desirable degree. Fig. 1b illustrates this loop.

Within this pipeline, new geometries are sampled by performing an adversarial attack that maximizes an adversarial loss such as

$$\max_{\delta \in \Delta} \mathcal{L}_{\text{adv}}(X, \delta; \theta) = \max_{\delta \in \Delta} \sigma_F^2(X_{\delta}). \quad (10)$$

In force-matching NN potentials, the uncertainty of the force may be a better descriptor of epistemic error than uncertainty in energy (see Supporting Information).

In the context of atomistic simulations, the perturbation δ is applied only to the nuclear coordinates, $X_{\delta} = (\mathbf{Z}, \mathbf{R} + \delta)$, $\delta \in \mathbb{R}^{n \times 3}$. For systems better described by collective variables (CVs) $\mathbf{s} = \mathbf{s}(\mathbf{R})$, an adversarial attack can be applied directly to these CVs,

$X_\delta = (\mathbf{Z}, \mathbf{s}^{-1}(\mathbf{s} + \boldsymbol{\delta}))$, as long as there is a differentiable function \mathbf{s}^{-1} mapping \mathbf{s} to the nuclear coordinates \mathbf{R} .

The set Δ can be defined by appropriately choosing ε , the maximum p -norm of δ . However, in atomistic simulations, it is often interesting to express these limits in terms of the energy of the states to be sampled, and the sampling temperature. To that end, a partition function Q of the system at a given temperature T can be constructed from the ground truth data \mathcal{D} ,

$$Q = \sum_{(X, E, \mathbf{F}) \in \mathcal{D}} \exp\left(-\frac{E}{kT}\right), \quad (11)$$

with k being the Boltzmann constant. Disregarding the entropic contributions, the probability p that a state X_δ with predicted energy $\bar{E}(X_\delta)$ will be sampled is

$$p(X_\delta) = \frac{1}{Q} \exp\left(-\frac{\bar{E}(X_\delta)}{kT}\right). \quad (12)$$

Finally, instead of limiting the norm of δ , the adversarial objective can be modified to limit the energy of sampled states by combining Eqs. (10) and (12),

$$\max_{\delta} \mathcal{L}_{\text{adv}}(X, \delta; \theta) = \max_{\delta} p(X_\delta) \sigma_F^2(X_\delta). \quad (13)$$

Using automatic differentiation strategies, the value of δ can be obtained by iteratively using gradient ascent techniques,

$$\delta^{(i+1)} = \delta^{(i)} + \alpha_\delta \frac{\partial \mathcal{L}_{\text{adv}}}{\partial \delta}, \quad (14)$$

with i the number of the iteration and α_δ the learning rate for the adversarial attack.

In practice, adversarial examples require input geometries as seeds, and an appropriate initialization of δ . One possibility is to sample the initial δ from a normal distribution $\mathcal{N}(0, \sigma_\delta^2 \mathbf{I})$ with a small value of σ_δ^2 . The degenerate case $\sigma_\delta^2 = 0$ leads to deterministic adversarial attacks with the optimization procedure.

Since one can create several adversarial examples per initial seed, the computational bottleneck becomes evaluating them to create more ground truth data. Hence, reducing the number of adversarial examples is of practical consideration. Generated examples can be reduced by using only a subset of the initial dataset \mathcal{D} as seeds. Even then, the optimization of δ may lead to structures which are very similar, corresponding to the same points in the configuration space. To avoid evaluating the same geometry multiple times, structures can be deduplicated according to the root mean square deviation (RMSD) between the conformers. One efficient algorithm is to perform hierarchical clustering on the data points given the RMSD matrix, and aggregating points which are within

a given threshold of each other. Finally, to avoid local minima around the training set, one can classify whether the given structure is well-known by the model using Eq. (8). Then, new points are evaluated only if they correspond to high uncertainty structures, avoiding sampling regions of the PES which are already well represented in the training set.

The complete adversarial training procedure is described in Algorithm 1.

Algorithm 1: Adversarial training of a neural network potential

Input: dataset \mathcal{D}_1 , hyperparameters

Data: geometries, energies and forces (X, E, \mathbf{F})

```

1 for generation  $g \in (1, \dots, G)$  do
  /* Training */
2   for model  $m \in (1, \dots, M)$  do
3     sample a train set from  $\mathcal{D}_g$ 
4     train  $h_\theta^{(m)}$  to minimize  $\mathcal{L}$  // Eqs. (2),(3)
  /* Adversarial Attack */
5   construct  $Q$  from  $\mathcal{D}_g$  // Eq. (11)
6
7   sample attack seeds  $\{X_i\}$  from  $\mathcal{D}_g$ 
8   for seed  $X_i \in \{X_i\}$  do
9     initialize  $\boldsymbol{\delta} \sim \mathcal{N}(0, \sigma_\delta^2 \mathbf{I})$ 
10    train  $\boldsymbol{\delta}$  to maximize  $\mathcal{L}_{\text{adv}}$  // Eqs. (13),(14)
11
12     $X_{\delta,i} := (\mathbf{Z}_i, \mathbf{R}_i + \boldsymbol{\delta})$ 
  /* Evaluating */
13  initialize  $\mathcal{D}_{g+1} := \mathcal{D}_g$ 
14  for adversarial example  $X_{\delta,i} \in \{X_{\delta,i}\}$  do
15    obtain ground-truth  $(E_{\delta,i}, \mathbf{F}_{\delta,i})$  for  $X_{\delta,i}$ 
16    add  $(X_{\delta,i}, E_{\delta,i}, \mathbf{F}_{\delta,i})$  to  $\mathcal{D}_{g+1}$ 

```

III. RESULTS AND DISCUSSION

A. Double well potential

As a proof-of-concept, the adversarial sampling strategy is demonstrated in the two-dimensional (2D) double well potential (see Supporting Information for a complete analysis of the 1D example). To investigate the exploration of the phase space, the initial data is placed randomly in one of the basins of the potential. Then, a committee of feedforward NNs is trained to reproduce the potential using the training data (see Methods). At first, the NN potential is unaware of the second basin, and predicts a single well potential in its first generation. As such, an MD simulation using this NN potential would be unable to reproduce the free energy surface of the true potential. Nevertheless, the region corresponding to the second basin is of high uncertainty when compared to the region where the training set is located. The adversarial loss encourages exploring the configuration space away from the original data, and adversarial samples that

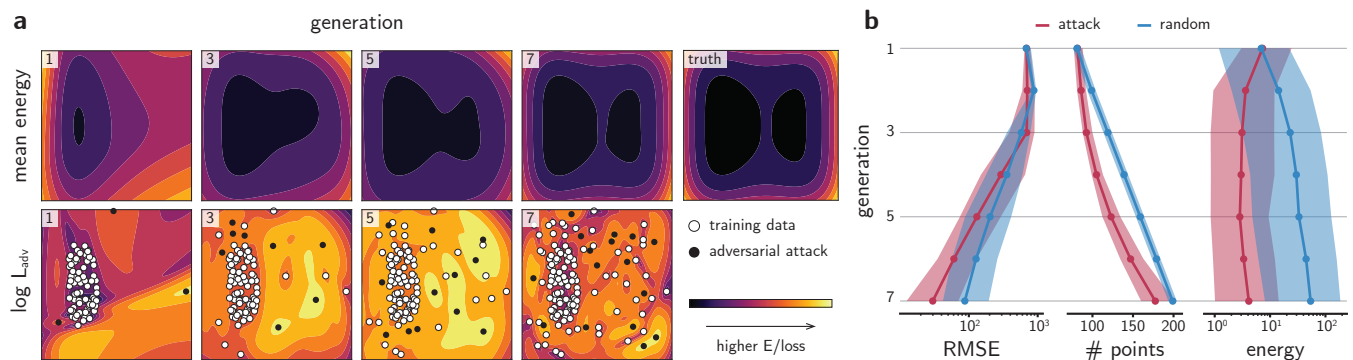


FIG. 2. **a**, Evolution of the PES of a 2D double well predicted by an NN committee. Adversarial examples (black dots) are distortions from original training data (white dots) or past adversarial examples (gray dots) that maximize the adversarial loss \mathcal{L}_{adv} . The plotting intervals are $[-1.5, 1.5] \times [-1.5, 1.5]$ for all graphs. The generation of the NN committee is shown in the top left corner of each graph. **b**, Evolution of the root mean square error (RMSE), number of training points and energy of the sampled points for adversarial attack strategy (red) and randomly distorting the training data (blue). The solid line is the median from more than 100 experiments, and the shaded area is the interquartile region.

maximize \mathcal{L}_{adv} are evaluated with the ground truth potential, then added to the training set of the next generation of NN potentials. Fig. 2a shows the results of the training-attacking loop for the NN potential after several generations. As the active learning loop proceeds, the phase space is explored just enough to accurately reproduce the 2D double well, including the energy barrier and the shape of the basins.

To verify the effectiveness of the adversarial sampling strategy, the evolution of the models is compared with a random sampling. While the former is obtained by solving Eq. (13), the latter is obtained by randomly selecting 20 different training points from the training set and sampling δ from a uniform distribution, $\delta \sim \mathcal{U}(-\sigma_\delta, \sigma_\delta)$. To perform a statistical analysis on the methods, more than 100 independent active learning loops with different initializations are trained for the same 2D well potential (Fig. 2b). Overall, the root mean square error (RMSE) between the ground truth potential and the predicted values decreases as the space is better sampled for both methods. However, although the random sampling strategy collects more data points, the median RMSE of the final generation is between two to three times higher than the adversarial attack strategy. Moreover, the median sampled energy is one order of magnitude higher for randomly-sampled points. As several randomly-sampled points travel to places outside of the bounds of the double well shown in Fig. 2a, the energy quickly increases, leading to high-energy configurations. This is often the case in real systems, in which randomly distorting molecules or solids rapidly lead to high-energy structures that will not be visited during production simulations. As such, this toy example suggests that the adversarial sampling method generates thermodynamically likely structures, requires less ground-truth evaluations and leads to better-trained NN potentials compared to randomly sampling the space.

B. Nitrogen inversion on ammonia

As a second example, we bootstrap an NN potential to study the nitrogen inversion in ammonia. This choice of molecule is motivated by more complex reactive systems, in which quantifying energy barriers to train a robust NN potential requires thousands of reactive trajectories from *ab initio* simulations.⁴² To circumvent that need, we start training an NN committee using the SchNet model²⁸ from Hessian-displaced geometries data. Then, new geometries are sampled by performing an adversarial attack on the ground state conformation, and later evaluated using DFT. After training a new committee with the new data points, the landscape of conformations is analyzed and compared with random displacements. Fig. 3a shows a UMAP visualization⁷⁸ of the conformers, as compared by their similarity using the Smooth Overlap of Atomic Positions (SOAP) representation.^{79,80} A qualitative analysis of the UMAP plot shows that adversarial attacks rarely resemble the training set in terms of geometric similarity. Attacks from the second generation are also mostly distant from attacks in the first generation. On the other hand, small values of distortions σ_δ for a uniform distribution (see Sec. III A) create geometries that are very similar to Hessian-displaced ones. While higher values of σ_δ (e.g. $\sigma_\delta = 0.3$ Å) explore a larger conformational space, several points with very high energy are sampled (Fig. 3b), as in the double well example. As the number of atoms increases, this trade-off between thermodynamic likelihood and diversity of the randomly sampled configurations worsens in a curse-of-dimensionality effect. In contrast, energies of adversarially-created conformations have a more reasonable upper bound. Fig. 3c compares the degree of distortion of the geometries with respect to their energies. It further shows that the adversarial strategy navigates the conformational space to find highly distorted,

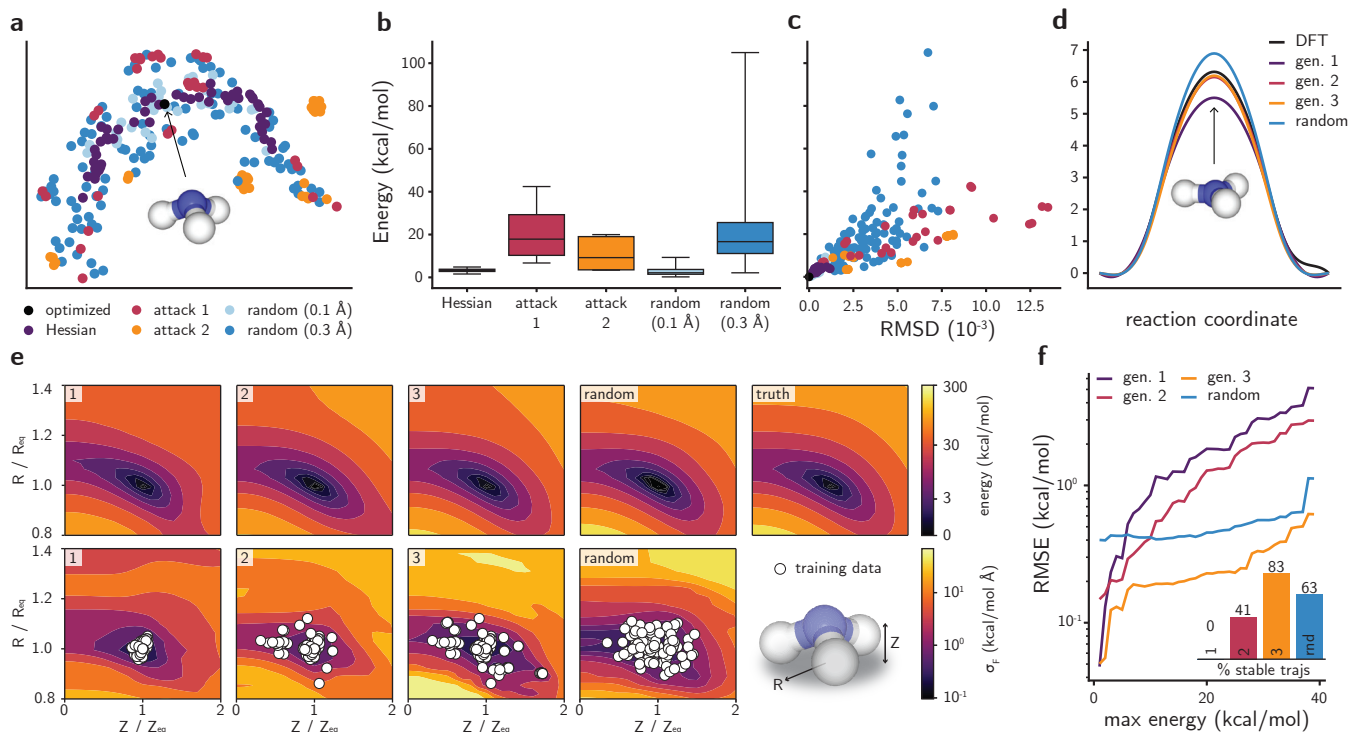


FIG. 3. **a**, UMAP plot for the SOAP-based similarity between ammonia geometries. Both axes are on the same scale. **b**, Distribution of DFT energies for conformations sampled with different methods. The horizontal line is the median, the box is the interquartile region and the whiskers span the range of the distribution. **c**, Relationship between DFT energy and root mean square deviation (RMSD) of a geometry with respect to the ground state structure of ammonia. The color scheme follows the legend of **a**. **d**, Energy barrier for the nitrogen inversion calculated with NEB using DFT or using the NN committee. **e**, Evolution of the ammonia PES with respect to the CVs R , Z . The generation of the NN committee is shown in the top left corner of each plot. The scale bar of energies is plotted with the function $\log_{10}(1 + E)$, and all energy contour plots have the same levels. Random geometries were generated with $\sigma_\delta = 0.3$ Å (see Methods). **f**, RMSE between the NN and DFT PES for each NN potential when a maximum energy is imposed for the DFT PES. **f**, inset, fraction of stable MD trajectories generated using each NN committee as force field.

lower energy states. Both the first and second generation of attacked geometries display higher RMSD than Hessian-displaced structures with respect to the ground state geometry while staying within reasonable energy bounds. However, as the low-energy region of the PES becomes better explored by the NN potential as the AL loop progresses, adversarially sampled geometries from later generations get increasingly higher in energy (Fig. S4).

Once new configurations are used in training, predictions for the energy barrier in the nitrogen inversion improve substantially (Fig. 3d). While the first generation of NN potential underestimates the energy barrier by about 1 kcal/mol with respect to the DFT value, the prediction from the second generation is already within the error bar, with less than 0.25 kcal/mol of error for the transformation (see Fig. S5). In contrast, predictions from an NN committee trained on randomly-sampled geometries overestimate the barrier. They also exhibit higher uncertainties, even for geometries close to equilibrium (Fig. S5). This suggests that the adversarial attack was able to sample geometries similar to the transition

state of the nitrogen inversion reaction and accurately interpolate the energy barrier without the need to manually add this reaction path into the training set.

The evolution of the phase space of each NN committee is further compared in Fig. 3e. Two CVs are defined to represent the phase space of this molecule: the radius of the circumference defined by the three hydrogen atoms (R) and the distance between the nitrogen atom and the plane defined by the three hydrogens (Z). Fig. 3e shows these CVs normalized by the values found in the ground state geometry. Analogously to Fig. 2a, adversarial attacks expand the configuration space used as train set for NN committees and bring the phase space closer to the ground truth, thus lowering the uncertainty of forces in the phase space. Nevertheless, randomly-sampled geometries also allow bootstrapping an NN committee depending on the system and values of σ_δ . Importantly, NN committees successively trained on adversarial attacks have smaller errors in the low-energy region of the PES of ammonia. As expected, the high-energy configurations sampled by randomly-generated geometries slightly improve the higher energy region of the PES that will not

be visited in production simulations. Fig. 3f shows the RMSE of each model compared to DFT across all the phase space of Fig. 3e. When only energies smaller than 5 kcal/mol are compared, all three generations display much smaller RMSE than random, probably due to the presence of Hessian-displaced geometries in their training set. The third generation of NN committees has a smaller RMSE when compared to random up to 40 kcal/mol, further supporting that the adversarial sampling strategy is useful to balance exploration of diverse conformations with higher likelihood. Finally, the adversarial training yields models capable of performing stable MD simulations. Whereas the first generation cannot produce stable MD trajectories, i.e. always leading to unphysical configurations such as atomic dissociation or collision, 83% of the trajectories produced by the third generation of adversarially based NN committees are stable, even though the NN-based MD geometries include data points originally not in the training set (Fig. S6). In contrast, only 63% of the trajectories are stable when the NN committee trained on random geometries is used. This indicates that the adversarial sampling strategy enhances the robustness of NN-based MD simulations by seeking points which are known to cause instabilities due to extrapolation errors.

C. Collective variable sampling in alanine dipeptide

As a final example, we illustrate the use of adversarial attacks for sampling predefined CVs. Since translation-based adversarial attacks $X_\delta = (\mathbf{Z}, \mathbf{R} + \delta)$ may not be able to capture collective dynamics of interest such as bond rotations, we seek to find conformations that increase the uncertainty of the NN potential in predefined CVs $\mathbf{s} = \mathbf{s}(\mathbf{R})$. To do that, there should exist a differentiable function \mathbf{s}^{-1} mapping a point in the CV space to the atomic coordinate space $\mathbb{R}^{n \times 3}$. Typically, CVs aggregate information from many degrees of freedom and $\mathbf{s}(\mathbf{R})$ may not be bijective. Nevertheless, in the case of adversarial attacks, it suffices to have an operation \mathbf{s}^{-1} that acts on a geometry $X = (\mathbf{Z}, \mathbf{R})$ to produce the adversarial attack $X_\delta = (\mathbf{Z}, \mathbf{s}^{-1}(X, \delta))$. Using this strategy, a seed geometry can be distorted in the direction of its predefined CVs even if the CVs are not invertible.

This application is illustrated with the alanine dipeptide (N-acetyl-L-alanine-N'-methylamide) molecule, using its two dihedral angles (φ, ψ) as CVs (Fig. 4a). In this particular case, the function \mathbf{s}^{-1} takes a reference geometry X as an input and performs the dihedral rotations of interest purely through geometrical operations. Since bond rotations can be written with matrix operations, they can be implemented in the training pipeline without breaking the computational graph that enables the adversarial strategy. To study the effects of the adversarial learning method, a series of NN committees were trained using the same architecture employed in the previous section. The models were trained on geometries

created from MD simulations using the Optimized Potentials for Liquid Simulations (OPLS) force field⁸¹ with the OpenMM package^{82,83} (see Methods). Then, adversarial attacks were performed by randomly taking training points as seed geometries. Since bond rotations are periodic, the adversarial distortion δ does not break the geometries apart, a concern that existed in the previous section or in many other ML-accelerated simulations. Nevertheless, some angles (φ, ψ) may lead to high energy configurations depending on the conformation X of the molecule prior to the attack. To avoid bounding the exploration of the phase space with the energy, Eq. (10) was used as the adversarial loss, and $\varepsilon = \pi$ radians. Fig. 4b shows the distribution of sampled energies for different rounds of adversarial attacks. We discarded points with extremely high energy from the training set, since they interfere with the training of the NN potential for being overly far from equilibrium. Nevertheless, the distribution of energies show that most of the sampled points lie in reasonable energy ranges typically not accessible by unbiased MD simulations. This further supports the hypothesis that adversarial attacks are effective in sampling regions of the phase space with good compromise between energy and uncertainty.

The evolution of NN committees for predicting the PES of alanine dipeptide is shown in Fig. 4c. At first, only a small region of the phase space is known from the data obtained in MD simulations. This is reflected on the high contrast between the uncertainty close and far from the training set. In the first few adversarial attacks, the space is better sampled according to the uncertainty metric, decreasing the uncertainty for $|\psi| > 0$ and increasing the uncertainty in high-energy regions. This suggests that the quality of the epistemic error classification improves as the conformation space is better explored. To better compare the ground truth results with the NN predictions in the low-energy region, we clipped the energies of the former to 300 kcal/mol in Fig. 4c. As the active learning loop progresses, the NN committee is able to better reproduce the energy landscape of alanine dipeptide, as exemplified by the improvement of the CV landscape for $\varphi > \pi/2$ or the high-energy ellipsoid centered at $(\varphi, \psi) = (0, 0)$. Interestingly, the uncertainty remains high in the central region, since the sampled energies of the system are much higher than the rest of the phase space. Since some of them are discarded for being extremely unlikely (e.g. configurations with energies greater than 10^4 kcal/mol), the predictive power of the NN committee is not guaranteed in this part of the phase space. This is characterized by the ring-like energy barrier featured in Fig. 4c for generations greater than 3. It is unclear whether NN potentials are able to simultaneously predict ground state conformations and such high energy states with similar absolute accuracy. In fact, learning high energy regions of the PES may not be needed, since the learned barriers are insurmountable in production simulations. Finally, the uncertainty in forces resembles traditional biasing potentials in enhanced sam-

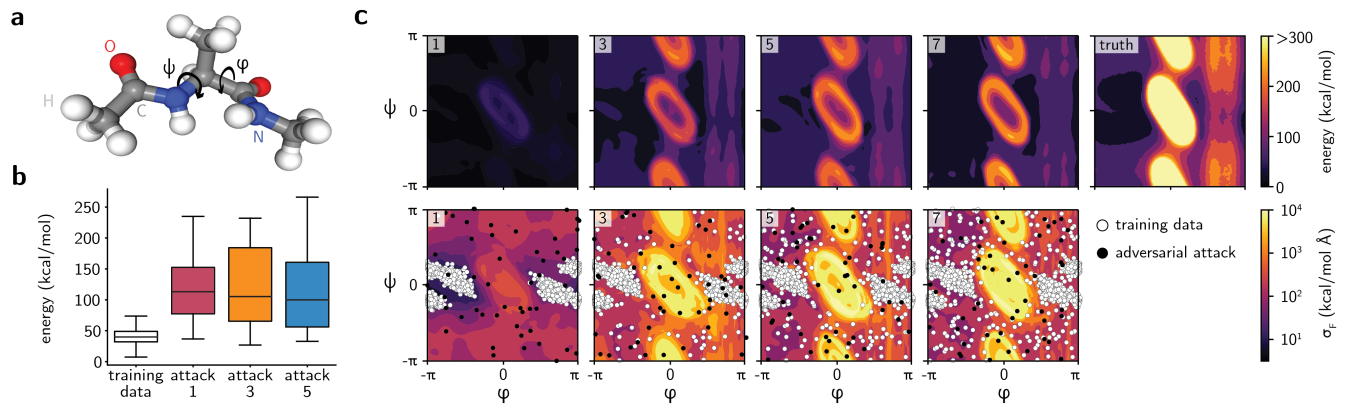


FIG. 4. **a**, Schematic diagram of alanine dipeptide and the CVs (φ , ψ) created from the highlighted dihedral angles. Hydrogen, carbon, oxygen and nitrogen atoms are depicted with white, gray, red and blue spheres, respectively. **b**, Distribution of force field energies for conformations generated from the collective variables. The horizontal line is the median, the box is the interquartile region and the whiskers span the range of the distribution. **c**, Evolution of the PES of an NN committee trained on alanine dipeptide. Adversarial examples (black dots) are distortions of the CVs (φ , ψ) from original training data (white dots) that maximize the forces variance σ_F^2 . Angles are given in radians.

pling techniques applied to obtain the free energy landscape in alanine dipeptide.^{84,85} Although this intuition is not thoroughly quantified in this work, we suggest that NN potentials with uncertainty quantification intrinsically provide a bias towards transition states through the uncertainty metric. Although the uncertainty can vary outside of the training set, as seen in Fig. 4c, this idea qualitatively agrees with the examples in this paper (see also Fig. S1a, S5). While we explore this bias through adversarial attacks for bootstrapping NN potentials in this work, we further suggest they could lead to automatic transition state and rare-event sampling strategies based on differentiable atomistic simulations. This opportunity will be explored in future works.

IV. CONCLUSIONS

In summary, we proposed a new sampling strategy for NN potentials by combining uncertainty quantification, adversarial attacks and active learning. By maximizing the uncertainty of NN predictions through a differentiable metric, new geometries can be sampled without the need for atomistic simulations. This technique allows NN potentials to be bootstrapped with less data without compromising the final accuracy, as well as efficient exploration of the conformational space. Adversarial attacks were demonstrated in three examples: a 2D double well potential, where it has provided an exploration strategy, outperforming a random baseline; an ammonia molecule, where it accurately predicted distorted configurations or reaction paths, as well as better fits to the PES and more stable atomistic simulations, without the need of AIMD; and the alanine dipeptide molecule, where adversarial attacks were performed on collective variables to efficiently explore the phase space. This work presents a

new way to train NN potentials and sample chemical conformations through deep learning-enabled simulations.

V. METHODS

A. Double well potential

The double well potential adopted in this work is written as the following polynomial:

$$E(x, y) = 10x^4 - 10x^2 + 2x + 4y^2. \quad (15)$$

Initial training data was generated by randomly sampling up to 800 points with independent coordinates according to a uniform distribution $\mathcal{U}(-1.5, 1.5)$, and selecting only those with energy lower than -2 . This allows us to select only data points lying in the lowest energy basin of the double well, creating an energy barrier between the two energy minima.

Five feedforward NNs with four layers, softplus activation and 1,024 units per layer were trained using the same train/test splits of the dataset. The NNs had different initial weights. The dataset was split in the ratio 60:20:20 for training : validation : testing, with a batch size of 35. The training was performed for 600 epochs with the Adam optimizer⁸⁶ and a learning rate of 0.001. The reported RMSE is the mean squared difference between the average predicted energy \bar{E} and the ground truth potential E as evaluated on a 100×100 grid in the interval $[-1.5, 1.5] \times [-1.5, 1.5]$.

Adversarial attacks were performed with a normalized sampling temperature of 5 (Eq. (15) units) for 600 epochs, learning rate of 0.003 and the Adam optimizer. Deduplication via hierarchical clustering was performed

using a threshold of 0.02 for the distance and the 80th percentile of the train set variance.

Random distortions were performed in each generation by displacing the (x, y) coordinates of training data points (or past random samples) by $\delta \sim \mathcal{U}(-1.0, 1.0)$. After deduplication via hierarchical clustering and uncertainty percentile as performed for adversarial attacks, up to 20 points were randomly selected from the resulting data. Distortions smaller than 1.0 were often unable to efficiently explore the PES of the double well, landing in the same basin.

B. Simulations of ammonia

Initial molecular conformers were generated using RDKit⁸⁷ with the MMFF94 force field.^{88,89} DFT structural optimizations and single-point calculations were performed using the BP86-D3/def2-SVP⁹⁰⁻⁹² level of theory as implemented in ORCA.^{93,94} NEB calculations⁹⁵⁻⁹⁷ were performed with 11 images using the FIRE algorithm⁹⁸ as implemented in the Atomic Simulation Environment.⁹⁹ Hessian-displaced geometries were created by randomly displacing the atoms from their ground state conformation in the direction of normal mode vectors with temperatures between 250 and 750 K. In total, 78 training geometries were used as initial dataset.

For each generation, five NNs with the SchNet architecture²⁸ were employed. Each model used four convolutions, 256 filters, atom basis of size 256, 32 learnable gaussians and cutoff of 5.0 Å. The models were trained on different splits of the initial dataset (ratios 60 : 20 : 20 for train : validation : test) for 500 epochs, using the Adam optimizer with an initial learning rate of 3×10^{-4} and batch size of 30. A scheduler reduced the learning rate by a factor of 0.5 if 30 epochs passed without improvement in the validation set. The training coefficients α_E and α_F (see Eq. 3) were set to 0.1 and 1, respectively.

Adversarial attacks were initialized by displacing the ground state geometry of ammonia by $\delta \sim \mathcal{N}(0, 0.01 \text{ Å})$ for each coordinate. The resulting attack δ was optimized for 60 iterations using the Adam optimizer with learning rate of 0.01. The normalized temperature kT was set to 20 kcal/mol to ensure that adversarial attacks were not bound by a low sampling temperature, but by the uncertainty in force predictions. 30 adversarial attacks were sampled for each generation. No deduplication was performed.

Random distortions were generated by displacing each coordinate of the ground state geometry of ammonia by a value of $\delta \sim \mathcal{U}(-\sigma_\delta, \sigma_\delta)$. The values of $\sigma_\delta = 0.1 \text{ Å}$ and $\sigma_\delta = 0.3 \text{ Å}$ were adopted. 30 (100) random samples were created for $\sigma_\delta = 0.3 \text{ Å}$ ($\sigma_\delta = 1.0 \text{ Å}$).

NN-based MD simulations were performed in the NVT ensemble with Nosé-Hoover dynamics¹⁰⁰, 0.5 fs timesteps, and temperatures of 500, 600, 700, 800, 900, and 1000 K. 100 5 ps-long trajectories were performed for each NN committee and temperature. The ground state

geometry of ammonia was used as initial configuration for all MD calculations. Trajectories were considered as unphysical if the distance between hydrogen atoms was closer than 0.80 Å or larger than 2.55 Å, or if the predicted energy was lower than the ground state energy (0 kcal/mol for the reference adopted in this work).

SOAP vectors were created using the DScribe package.¹⁰¹ The cutoff radius was set as 5 Å, with spherical primitive gaussian type orbitals with standard deviation of 1 Å, basis size of 5 functions, and $L_{\max} = 6$. The vectors were averaged over sites before summing the magnetic quantum numbers.

C. Simulations of alanine dipeptide

Alanine dipeptide was simulated using the OPLS force field⁸¹ within the OpenMM simulation package.^{82,83} The force field parameters were generated using LigParGen.¹⁰² The molecule was placed in vacuum, with a box of size 15 Å. MD simulations were performed at 300 K using a Langevin integrator with a friction coefficient of 1 ps^{-1} and step sizes of 2 fs. Calculations of Lennard-Jones and Coulomb interactions were performed in real space with no cutoff. The initial training data was obtained by conducting 2 ns of MD simulations, from which snapshots every 2 ps were collected.

For each generation, five NNs with the SchNet architecture²⁸ were employed. The NNs follow the same architecture employed in the simulation of ammonia (see V B). The models were trained for 500 epochs, using the Adam optimizer with an initial learning rate of 5×10^{-4} , batch size of 50, and learning rate scheduler. The training coefficients α_E and α_F (see Eq. 3) were both set to 1.0.

Adversarial attacks were initialized by displacing the CVs (φ, ψ) by $\delta \sim \mathcal{N}(0, 0.01 \text{ rad})$ for each angle. The resulting attack δ was optimized for 1000 iterations using the Adam optimizer with learning rate of 5×10^{-3} . Eq. (10) was used without bounds for δ . 50 adversarial attacks were sampled for each generation. No deduplication was performed.

ACKNOWLEDGEMENTS

D.S.-K. acknowledges the MIT Energy Fellowship for financial support. A.R.T. thanks Asahi Glass Company for financial support.

REFERENCES

- ¹K. T. Butler, D. W. Davies, H. Cartwright, O. Isayev, and A. Walsh, "Machine learning for molecular and materials science," *Nature* **559**, 547–555 (2018).

- ²B. Sanchez-Lengeling and A. Aspuru-Guzik, "Inverse molecular design using machine learning: Generative models for matter engineering," *Science* **361**, 360–365 (2018).
- ³A. Zunger, "Inverse design in search of materials with target functionalities," *Nature Reviews Chemistry* **2**, 0121 (2018).
- ⁴J. Schmidt, M. R. G. Marques, S. Botti, and M. A. L. Marques, "Recent advances and applications of machine learning in solid-state materials science," *npj Computational Materials* **5**, 83 (2019).
- ⁵O. A. von Lilienfeld, K.-R. Müller, and A. Tkatchenko, "Exploring chemical compound space with quantum-based machine learning," *Nature Reviews Chemistry* **4**, 347–358 (2020).
- ⁶D. Schwalbe-Koda and R. Gómez-Bombarelli, "Generative Models for Automatic Chemical Design," in *Lecture Notes in Physics*, Vol. 968 (Springer, 2020) pp. 445–467.
- ⁷J. Behler, "Neural network potential-energy surfaces in chemistry: a tool for large-scale simulations," *Physical Chemistry Chemical Physics* **13**, 17930 (2011).
- ⁸J. Behler, "Constructing high-dimensional neural network potentials: A tutorial review," *Int. J. Quantum Chem.* **115**, 1032 (2015).
- ⁹V. Botu, R. Batra, J. Chapman, and R. Ramprasad, "Machine learning force fields: Construction, validation, and outlook," *Journal of Physical Chemistry C* **121**, 511–522 (2017).
- ¹⁰V. L. Deringer, M. A. Caro, and G. Csányi, "Machine Learning Interatomic Potentials as Emerging Tools for Materials Science," *Advanced Materials* **31**, 1902765 (2019).
- ¹¹S. Manzhos and T. Carrington, "Neural Network Potential Energy Surfaces for Small Molecules and Reactions," *Chemical Reviews* (2020), 10.1021/acs.chemrev.0c00665.
- ¹²T. Mueller, A. Hernandez, and C. Wang, "Machine learning for interatomic potential models," *The Journal of Chemical Physics* **152**, 50902 (2020).
- ¹³A. P. Bartók, M. C. Payne, R. Kondor, and G. Csányi, "Gaussian Approximation Potentials: The Accuracy of Quantum Mechanics, without the Electrons," *Physical Review Letters* **104**, 136403 (2010).
- ¹⁴M. Rupp, A. Tkatchenko, K.-R. Müller, and O. A. von Lilienfeld, "Fast and Accurate Modeling of Molecular Atomization Energies with Machine Learning," *Physical Review Letters* **108**, 58301 (2012).
- ¹⁵A. P. Thompson, L. P. Swiler, C. R. Trott, S. M. Foiles, and G. J. Tucker, "Spectral neighbor analysis method for automated generation of quantum-accurate interatomic potentials," *Journal of Computational Physics* **285**, 316–330 (2015).
- ¹⁶Z. Li, J. R. Kermode, and A. De Vita, "Molecular Dynamics with On-the-Fly Machine Learning of Quantum-Mechanical Forces," *Physical Review Letters* **114**, 096405 (2015).
- ¹⁷A. P. Bartók, S. De, C. Poelking, N. Bernstein, J. R. Kermode, G. Csányi, and M. Ceriotti, "Machine learning unifies the modeling of materials and molecules," *Science Advances* **3**, e1701816 (2017).
- ¹⁸S. Chmiela, A. Tkatchenko, H. E. Sauceda, I. Poltavsky, K. T. Schütt, and K.-R. Müller, "Machine learning of accurate energy-conserving molecular force fields," *Science Advances* **3**, e1603015 (2017).
- ¹⁹S. Chmiela, H. E. Sauceda, K.-R. Müller, and A. Tkatchenko, "Towards exact molecular dynamics simulations with machine-learned force fields," *Nature Communications* **9**, 3887 (2018).
- ²⁰A. V. Shapeev, "Moment tensor potentials: A class of systematically improvable interatomic potentials," *Multiscale Modeling and Simulation* **14**, 1153–1173 (2016).
- ²¹A. Glielmo, C. Zeni, and A. De Vita, "Efficient nonparametric N -body force fields from machine learning," *Physical Review B* **97**, 184307 (2018).
- ²²J. Vandermause, S. B. Torrisi, S. Batzner, Y. Xie, L. Sun, A. M. Kolpak, and B. Kozinsky, "On-the-fly active learning of interpretable Bayesian force fields for atomistic rare events," *npj Computational Materials* **6**, 20 (2020).
- ²³H. Liu, Y.-S. Ong, X. Shen, and J. Cai, "When Gaussian Process Meets Big Data: A Review of Scalable GPs," *IEEE Transactions on Neural Networks and Learning Systems* **31**, 4405–4423 (2018).
- ²⁴J. Behler and M. Parrinello, "Generalized neural-network representation of high-dimensional potential-energy surfaces," *Physical Review Letters* **98**, 146401 (2007).
- ²⁵J. Behler, "Atom-centered symmetry functions for constructing high-dimensional neural network potentials," *The Journal of Chemical Physics* **134**, 074106 (2011).
- ²⁶N. Artrith and A. M. Kolpak, "Understanding the composition and activity of electrocatalytic nanoalloys in aqueous solvents: A combination of DFT and accurate neural network potentials," *Nano Letters* **14**, 2670–2676 (2014).
- ²⁷K. T. Schütt, F. Arbabzadah, S. Chmiela, K. R. Müller, and A. Tkatchenko, "Quantum-chemical insights from deep tensor neural networks," *Nature Communications* **8**, 6–13 (2017).
- ²⁸K. T. Schütt, H. E. Sauceda, P.-J. J. Kindermans, A. Tkatchenko, and K.-R. R. Müller, "SchNet - A deep learning architecture for molecules and materials," *Journal of Chemical Physics* **148**, 241722 (2018).
- ²⁹J. S. Smith, O. Isayev, and A. E. Roitberg, "ANI-1: an extensible neural network potential with DFT accuracy at force field computational cost," *Chemical Science* **8**, 3192–3203 (2017).
- ³⁰L. Zhang, J. Han, H. Wang, R. Car, and E. Weinan, "Deep Potential Molecular Dynamics: A Scalable Model with the Accuracy of Quantum Mechanics," *Physical Review Letters* **120**, 143001 (2018).
- ³¹O. T. Unke and M. Meuwly, "PhysNet: A Neural Network for Predicting Energies, Forces, Dipole Moments, and Partial Charges," *Journal of Chemical Theory and Computation* **15**, 3678–3693 (2019).
- ³²J. Klicpera, J. Groß, and S. Günnemann, "Directional message passing for molecular graphs," in *ICLR* (2020) pp. 1–13.
- ³³K. V. J. Jose, N. Artrith, and J. Behler, "Construction of high-dimensional neural network potentials using environment-dependent atom pairs," *The Journal of Chemical Physics* **136**, 194111 (2012).
- ³⁴T. Morawietz, V. Sharma, and J. Behler, "A neural network potential-energy surface for the water dimer based on environment-dependent atomic energies and charges," *The Journal of Chemical Physics* **136**, 64103 (2012).
- ³⁵M. Gastegger, C. Kauffmann, J. Behler, and P. Marquetand, "Comparing the accuracy of high-dimensional neural network potentials and the systematic molecular fragmentation method: A benchmark study for all-trans alkanes," *The Journal of Chemical Physics* **144**, 194110 (2016).
- ³⁶T. Morawietz, A. Singraber, C. Dellago, and J. Behler, "How van der Waals interactions determine the unique properties of water," *Proceedings of the National Academy of Sciences* **113**, 8368 LP – 8373 (2016).
- ³⁷J. Behler, R. Martoňák, D. Donadio, and M. Parrinello, "Metadynamics Simulations of the High-Pressure Phases of Silicon Employing a High-Dimensional Neural Network Potential," *Physical Review Letters* **100**, 185501 (2008).
- ³⁸N. Artrith, T. Morawietz, and J. Behler, "High-dimensional neural-network potentials for multicomponent systems: Applications to zinc oxide," *Physical Review B* **83**, 153101 (2011).
- ³⁹N. Artrith and A. Urban, "An implementation of artificial neural-network potentials for atomistic materials simulations: Performance for TiO₂," *Computational Materials Science* **114**, 135–150 (2016).
- ⁴⁰S. K. Natarajan and J. Behler, "Neural network molecular dynamics simulations of solid–liquid interfaces: water at low-index copper surfaces," *Phys. Chem. Chem. Phys.* **18**, 28704–28725 (2016).
- ⁴¹M. Gastegger and P. Marquetand, "High-Dimensional Neural Network Potentials for Organic Reactions and an Improved Training Algorithm," *Journal of Chemical Theory and Computation* **11**, 2187–2198 (2015).

- ⁴²S. J. Ang, W. Wang, D. Schwalbe-koda, S. Axelrod, and R. Gómez-Bombarelli, "Active Learning Accelerates Ab Initio Molecular Dynamics on Pericyclic Reactive Energy Surfaces," *ChemRxiv.11910948.v2*, 1–32 (2020).
- ⁴³R. Z. Khaliullin, H. Eshet, T. D. Kühne, J. Behler, and M. Parrinello, "Nucleation mechanism for the direct graphite-to-diamond phase transition," *Nature Materials* **10**, 693–697 (2011).
- ⁴⁴H. Niu, L. Bonati, P. M. Piaggi, and M. Parrinello, "Ab initio phase diagram and nucleation of gallium," *Nature Communications* **11**, 2654 (2020).
- ⁴⁵B. Cheng, G. Mazzola, C. J. Pickard, and M. Ceriotti, "Evidence for supercritical behaviour of high-pressure liquid hydrogen," *Nature* **585**, 217–220 (2020).
- ⁴⁶V. L. Deringer, N. Bernstein, G. Csányi, C. Ben Mahmoud, M. Ceriotti, M. Wilson, D. A. Drabold, and S. R. Elliott, "Origins of structural and electronic transitions in disordered silicon," *Nature* **589**, 59–64 (2021).
- ⁴⁷D. Barrett, F. Hill, A. Santoro, A. Morcos, and T. Lillicrap, "Measuring abstract reasoning in neural networks," in *Proceedings of the 35th International Conference on Machine Learning*, Proceedings of Machine Learning Research, Vol. 80, edited by J. Dy and A. Krause (PMLR, Stockholmsmässan, Stockholm Sweden, 2018) pp. 511–520.
- ⁴⁸K. Xu, J. Li, M. Zhang, S. S. Du, K.-i. Kawarabayashi, and S. Jegelka, "How neural networks extrapolate: From feedforward to graph neural networks," *arXiv:2009.11848* (2020).
- ⁴⁹W. Wang, T. Yang, W. H. Harris, R. Gómez-Bombarelli, R. Gomez-Bombarelli, and R. Gómez-Bombarelli, "Active learning and neural network potentials accelerate molecular screening of ether-based solvate ionic liquids," *Chemical Communications* **56**, 8920–8923 (2020).
- ⁵⁰A. A. Peterson, R. Christensen, and A. Khorshidi, "Addressing uncertainty in atomistic machine learning," *Physical Chemistry Chemical Physics* **19**, 10978–10985 (2017).
- ⁵¹F. Musil, M. J. Willatt, M. A. Langovoy, M. Ceriotti, M. J. Willatt, M. A. Langovoy, and M. Ceriotti, "Fast and Accurate Uncertainty Estimation in Chemical Machine Learning," *Journal of Chemical Theory and Computation* **15**, 906–915 (2019).
- ⁵²K. Tran, W. Neiswanger, J. Yoon, Q. Zhang, E. Xing, and Z. W. Ulissi, "Methods for comparing uncertainty quantifications for material property predictions," *Machine Learning: Science and Technology* **1**, 025006 (2020).
- ⁵³S. Venturi, R. L. Jaffe, and M. Panesi, "Bayesian Machine Learning Approach to the Quantification of Uncertainties on Ab Initio Potential Energy Surfaces," *Journal of Physical Chemistry A* **124**, 5129–5146 (2020).
- ⁵⁴R. Jinnouchi, J. Lahnsteiner, F. Karsai, G. Kresse, and M. Bokdam, "Phase Transitions of Hybrid Perovskites Simulated by Machine-Learning Force Fields Trained on the Fly with Bayesian Inference," *Physical Review Letters* **122**, 225701 (2019).
- ⁵⁵J. A. Garrido Torres, P. C. Jennings, M. H. Hansen, J. R. Boes, and T. Bligaard, "Low-Scaling Algorithm for Nudged Elastic Band Calculations Using a Surrogate Machine Learning Model," *Physical Review Letters* **122**, 156001 (2019).
- ⁵⁶C. Blundell, J. Cornebise, K. Kavukcuoglu, and D. Wierstra, "Weight Uncertainty in Neural Network," in *Proceedings of the 32nd International Conference on Machine Learning*, Proceedings of Machine Learning Research, Vol. 37, edited by F. Bach and D. Blei (PMLR, Lille, France, 2015) pp. 1613–1622.
- ⁵⁷Y. Gal and Z. Ghahramani, "Dropout as a Bayesian Approximation: Representing Model Uncertainty in Deep Learning," in *Proceedings of The 33rd International Conference on Machine Learning*, Proceedings of Machine Learning Research, Vol. 48, edited by M. F. Balcan and K. Q. Weinberger (PMLR, New York, New York, USA, 2016) pp. 1050–1059.
- ⁵⁸D. N. Politis and J. P. Romano, "Large Sample Confidence Regions Based on Subsamples under Minimal Assumptions," *Ann. Statist.* **22**, 2031–2050 (1994).
- ⁵⁹R. T. Clemen, "Combining forecasts: A review and annotated bibliography," *International Journal of Forecasting* **5**, 559–583 (1989).
- ⁶⁰L. K. Hansen and P. Salamon, "Neural network ensembles," *IEEE Transactions on Pattern Analysis and Machine Intelligence* **12**, 993–1001 (1990).
- ⁶¹Y. Zhao, N. E. Schultz, and D. G. Truhlar, "Exchange-correlation functional with broad accuracy for metallic and non-metallic compounds, kinetics, and noncovalent interactions," (2005).
- ⁶²J. Behler, "Representing potential energy surfaces by high-dimensional neural network potentials," *Journal of Physics: Condensed Matter* **26**, 183001 (2014).
- ⁶³L. Chen, I. Sukuba, M. Probst, A. Kaiser, I. Sukuba, and M. Probst, "Iterative training set refinement enables reactive molecular dynamics: Via machine learned forces," *RSC Advances* **10**, 4293–4299 (2020).
- ⁶⁴C. Schran, K. Brezina, and O. Marsalek, "Committee neural network potentials control generalization errors and enable active learning," *Journal of Chemical Physics* **153**, 104105 (2020).
- ⁶⁵G. Imbalzano, Y. Zhuang, V. Kapil, K. Rossi, E. A. Engel, F. Grasselli, and M. Ceriotti, "Uncertainty estimation by committee models for molecular dynamics and thermodynamic averages," *arXiv:2011.08828*, 30–35 (2020).
- ⁶⁶A. Shapeev, K. Gubaev, E. Tsymbalov, and E. Podryabinkin, "Active Learning and Uncertainty Estimation," in *Machine Learning Meets Quantum Physics*, edited by K. T. Schütt, S. Chmiela, O. A. von Lilienfeld, A. Tkatchenko, K. Tsuda, and K.-R. Müller (Springer International Publishing, Cham, 2020) pp. 309–329.
- ⁶⁷Q. Lin, Y. Zhang, B. Zhao, and B. Jiang, "Automatically growing global reactive neural network potential energy surfaces: A trajectory-free active learning strategy," *Journal of Chemical Physics* **152**, 154104 (2020).
- ⁶⁸F. Noé, S. Olsson, J. Köhler, and H. Wu, "Boltzmann generators: Sampling equilibrium states of many-body systems with deep learning," *Science* **365**, eaaw1147 (2019).
- ⁶⁹W. Wang, S. Axelrod, and R. Gómez-Bombarelli, "Differentiable Molecular Simulations for Control and Learning," *arXiv:2003.00868* (2020).
- ⁷⁰C. Szegedy, A. Toshev, and D. Erhan, "Deep Neural Networks for Object Detection," undefined (2013).
- ⁷¹I. J. Goodfellow, J. Shlens, and C. Szegedy, "Explaining and harnessing adversarial examples," 3rd International Conference on Learning Representations, ICLR 2015 - Conference Track Proceedings, 1–11 (2015).
- ⁷²S. Rudner, "An overview of gradient descent optimization algorithms," *arXiv:1609.04747* (2016).
- ⁷³D. Tsipras, S. Santurkar, L. Engstrom, A. Turner, A. Madry, and A. Madry, "Robustness May Be at Odds with Accuracy," in *International Conference on Learning Representations* (2018) pp. 161–168.
- ⁷⁴C. Szegedy, W. Zaremba, I. Sutskever, J. Bruna, D. Erhan, I. Goodfellow, and R. Fergus, "Intriguing properties of neural networks," 2nd International Conference on Learning Representations, ICLR 2014 - Conference Track Proceedings, 1–10 (2014).
- ⁷⁵M. Ducoffe and F. Precioso, "Adversarial Active Learning for Deep Networks: a Margin Based Approach," *arXiv:1802.09841* (2018).
- ⁷⁶D. Zügner, A. Akbarnejad, and S. Günnemann, "Adversarial Attacks on Neural Networks for Graph Data," in *Proceedings of the 24th ACM SIGKDD International Conference on Knowledge Discovery & Data Mining*, KDD '18 (Association for Computing Machinery, New York, NY, USA, 2018) p. 2847–2856.
- ⁷⁷D. Zhu, Z. Zhang, P. Cui, and W. Zhu, "Robust Graph Convolutional Networks Against Adversarial Attacks," in *Proceedings of the 25th ACM SIGKDD International Conference on Knowledge Discovery & Data Mining*, KDD '19 (Associa-

- tion for Computing Machinery, New York, NY, USA, 2019) p. 1399–1407.
- ⁷⁸L. McInnes, J. Healy, N. Saul, and L. Großberger, “UMAP: Uniform Manifold Approximation and Projection,” *Journal of Open Source Software* **3**, 861 (2018).
 - ⁷⁹A. P. Bartók, R. Kondor, and G. Csányi, “On representing chemical environments,” *Physical Review B* **87**, 184115 (2013).
 - ⁸⁰S. De, A. P. Bartók, G. Csányi, and M. Ceriotti, “Comparing molecules and solids across structural and alchemical space,” *Physical Chemistry Chemical Physics* **18**, 13754–13769 (2016).
 - ⁸¹M. J. Robertson, J. Tirado-Rives, and W. L. Jorgensen, “Improved Peptide and Protein Torsional Energetics with the OPLS-AA Force Field,” *Journal of Chemical Theory and Computation* **11**, 3499–3509 (2015).
 - ⁸²M. S. Friedrichs, P. Eastman, V. Vaidyanathan, M. Houston, S. Legrand, A. L. Beberg, D. L. Ensign, C. M. Bruns, and V. S. Pande, “Accelerating molecular dynamic simulation on graphics processing units,” *Journal of Computational Chemistry* **30**, 864–872 (2009).
 - ⁸³P. Eastman, J. Swails, J. D. Chodera, R. T. McGibbon, Y. Zhao, K. A. Beauchamp, L.-P. Wang, A. C. Simmonett, M. P. Harrigan, C. D. Stern, R. P. Wiewiora, B. R. Brooks, and V. S. Pande, “OpenMM 7: Rapid development of high performance algorithms for molecular dynamics,” *PLOS Computational Biology* **13**, e1005659 (2017).
 - ⁸⁴A. Laio and M. Parrinello, “Escaping free-energy minima,” *Proceedings of the National Academy of Sciences* **99**, 12562–12566 (2002).
 - ⁸⁵J. Zhang, Y. I. Yang, and F. Noé, “Targeted Adversarial Learning Optimized Sampling,” *Journal of Physical Chemistry Letters* **10**, 5791–5797 (2019).
 - ⁸⁶D. P. Kingma and J. L. Ba, “Adam: A method for stochastic optimization,” 3rd International Conference on Learning Representations, ICLR 2015 - Conference Track Proceedings , 1–15 (2015).
 - ⁸⁷G. Landrum, “RDKit: Open-source cheminformatics,” (2006).
 - ⁸⁸T. A. Halgren, “Merck molecular force field. I. Basis, form, scope, parameterization, and performance of MMFF94,” *Journal of Computational Chemistry* **17**, 490–519 (1996).
 - ⁸⁹P. Tosco, N. Stiefl, and G. Landrum, “Bringing the MMFF force field to the RDKit: implementation and validation,” *Journal of Cheminformatics* **6** (2014), 10.1186/s13321-014-0037-3.
 - ⁹⁰Becke and A. D. Becke, “Density-functional exchange-energy approximation with correct asymptotic behavior,” *Physical Review A* **38**, 3098–3100 (1988).
 - ⁹¹J. P. Perdew, “Density-functional approximation for the correlation energy of the inhomogeneous electron gas,” *Physical Review B* **33**, 8822–8824 (1986).
 - ⁹²F. Weigend and R. Ahlrichs, “Balanced basis sets of split valence, triple zeta valence and quadruple zeta valence quality for H to Rn: Design and assessment of accuracy,” *Physical Chemistry Chemical Physics* **7**, 3297–3305 (2005).
 - ⁹³F. Neese, “The ORCA program system,” *Wiley Interdisciplinary Reviews: Computational Molecular Science* **2**, 73–78 (2012).
 - ⁹⁴F. Neese, “Software update: the ORCA program system, version 4.0,” *WIREs Computational Molecular Science* **8**, e1327 (2018).
 - ⁹⁵H. Jónsson, G. Mills, and K. W. Jacobsen, “Nudged elastic band method for finding minimum energy paths of transitions,” in *Classical and Quantum Dynamics in Condensed Phase Simulations* (WORLD SCIENTIFIC, 1998) pp. 385–404.
 - ⁹⁶G. Henkelman, B. P. Uberuaga, and H. Jónsson, “Climbing image nudged elastic band method for finding saddle points and minimum energy paths,” *Journal of Chemical Physics* **113**, 9901–9904 (2000).
 - ⁹⁷G. Henkelman and H. Jónsson, “Improved tangent estimate in the nudged elastic band method for finding minimum energy paths and saddle points,” *The Journal of Chemical Physics* **113**, 9978–9985 (2000).
 - ⁹⁸E. Bitzek, P. Koskinen, F. Gähler, M. Moseler, and P. Gumbsch, “Structural relaxation made simple,” *Physical Review Letters* **97**, 170201 (2006).
 - ⁹⁹A. Hjorth Larsen, J. Jørgen Mortensen, J. Blomqvist, I. E. Castelli, R. Christensen, M. Dulak, J. Friis, M. N. Groves, B. Hammer, C. Hargus, E. D. Hermes, P. C. Jennings, P. Bjerre Jensen, J. Kermode, J. R. Kitchin, E. Leonhard Kolsbjerg, J. Kubal, K. Kaasbjerg, S. Lysgaard, J. Bergmann Maronsson, T. Maxson, T. Olsen, L. Pastewka, A. Peterson, C. Rossgaard, J. Schiøtz, O. Schütt, M. Strange, K. S. Thygesen, T. Vegge, L. Vilhelmsen, M. Walter, Z. Zeng, and K. W. Jacobsen, “The atomic simulation environment—a Python library for working with atoms,” *Journal of Physics: Condensed Matter* **29**, 273002 (2017).
 - ¹⁰⁰S. Melchionna, G. Ciccotti, and B. L. Holian, “Hoover NPT dynamics for systems varying in shape and size,” *Molecular Physics* **78**, 533–544 (1993).
 - ¹⁰¹L. Himanen, M. O. J. Jäger, E. V. Morooka, F. Federici Canova, Y. S. Ranawat, D. Z. Gao, P. Rinke, and A. S. Foster, “DScribe: Library of descriptors for machine learning in materials science,” *Computer Physics Communications* **247**, 106949 (2020).
 - ¹⁰²L. S. Dodda, I. Cabeza de Vaca, J. Tirado-Rives, W. L. Jorgensen, I. Cabeza de Vaca, J. Tirado-Rives, and W. L. Jorgensen, “LigParGen web server: an automatic OPLS-AA parameter generator for organic ligands,” *Nucleic Acids Research* **45**, W331–W336 (2017).